Implementation of Topological Quantum Gates in Magnet-Superconductor Hybrid Structures
Supplemental Material

Jasmin Bedow[1], Eric Mascot[2], Themba Hodge[2], Stephan Rachel[2] and Dirk K. Morr[1]

[1] *Department of Physics, University of Illinois at Chicago, Chicago, IL 60607, USA*

[2] *School of Physics, University of Melbourne, Parkville, VIC 3010, Australia*

SUPPLEMENTARY SECTION 1: THEORETICAL FORMALISM

A. Construction of ground-state wave-functions

The Hamiltonian in Eq. (1) of the main text can be recast into the Bogoliubov de Gennes (BdG) form

$$\mathcal{H}(t) = \frac{1}{2}\sum_{i,j} \begin{pmatrix} c_i^\dagger & c_i \end{pmatrix} \underbrace{\begin{pmatrix} H_{ij}(t) & \Delta_{ij} \\ \Delta^*_{ji} & -H^*_{ij}(t) \end{pmatrix}}_{H_{\mathrm{BdG}}} \begin{pmatrix} c_j \\ c_j^\dagger \end{pmatrix}, \tag{S1}$$

with H_{BdG} possessing a particle-hole symmetry, as reflected in $H_{\mathrm{BdG}} = -\tau_x H^*_{\mathrm{BdG}} \tau_x$, where τ_x is a Pauli matrix. At $t = 0$, the Bogoliubov transformation,

$$\begin{pmatrix} c_j \\ c_j^\dagger \end{pmatrix} = \sum_n \begin{pmatrix} U_{jn} & V^*_{jn} \\ V_{jn} & U^*_{jn} \end{pmatrix} \begin{pmatrix} d_n \\ d_n^\dagger \end{pmatrix}, \tag{S2}$$

diagonalizes the Hamiltonian as

$$\mathcal{H}(0) = \sum_n E_n \left(d_n^\dagger d_n - \frac{1}{2} \right), \tag{S3}$$

where $E_n \geq 0$. The ground state is the quasiparticle vacuum, $|\Omega\rangle$, such that $d_n |\Omega\rangle = 0$ for all n. We construct the quasiparticle vacuum as a product state [1–3]. This is done by annihilating all quasiparticles from the true c-particle vacuum.

$$|\Omega\rangle = \frac{1}{\sqrt{\mathcal{N}}} d_1 \dots d_N |0\rangle . \tag{S4}$$

The normalization is given by $\mathcal{N} = |\det(V)|$. The degenerate ground states are thus

$$\begin{aligned} |00\rangle &= |\Omega\rangle , \\ |01\rangle &= d_2^\dagger |\Omega\rangle , \\ |10\rangle &= d_1^\dagger |\Omega\rangle , \\ |11\rangle &= d_1^\dagger d_2^\dagger |\Omega\rangle . \end{aligned} \tag{S5}$$

B. Time evolution of states

We define

$$d_n(t) = \mathcal{U}(t) d_n \mathcal{U}^{-1}(t) \tag{S6}$$

where $\mathcal{U}(t)$ is the unitary time-evolution operator,

$$\mathcal{U}(t) = \mathcal{T} \exp\left[-\frac{\mathrm{i}}{\hbar} \int_0^t dt' \mathcal{H}(t') \right] . \tag{S7}$$

Using the time-dependent BdG equations [4–6], the time-evolved operators are given by

$$\begin{pmatrix} d_n^\dagger(t) & d_n(t) \end{pmatrix} = \sum_i \begin{pmatrix} c_i^\dagger & c_i \end{pmatrix} \begin{pmatrix} U_{in}(t) & V_{in}^*(t) \\ V_{in}(t) & U_{in}^*(t) \end{pmatrix}, \tag{S8}$$

where

$$\begin{pmatrix} U(t) & V^*(t) \\ V(t) & U^*(t) \end{pmatrix} = \mathcal{T} \exp\left[-\frac{\mathrm{i}}{\hbar}\int_0^t dt' H_{\mathrm{BdG}}(t')\right] \begin{pmatrix} U & V^* \\ V & U^* \end{pmatrix}. \tag{S9}$$

We can now write the time-evolved ground states

$$\begin{aligned} |00(t)\rangle &= |\Omega(t)\rangle , \\ |01(t)\rangle &= d_2^\dagger(t) |\Omega(t)\rangle , \\ |10(t)\rangle &= d_1^\dagger(t) |\Omega(t)\rangle , \\ |11(t)\rangle &= d_1^\dagger(t) d_2^\dagger(t) |\Omega(t)\rangle . \end{aligned} \tag{S10}$$

The time-evolved quasiparticle vacuum is given by

$$|\Omega(t)\rangle = \frac{e^{\mathrm{i}\alpha(t)}}{\sqrt{\mathcal{N}(t)}} \prod_k d_k(t) |0\rangle . \tag{S11}$$

The normalization is given by $\mathcal{N}(t) = |\det(V(t))|$. The phase $\alpha(t)$ arises from the evolution of the true vacuum. However, this phase is gauged away in our gauge-invariant formulation of physical quantities, such as the geometric phase.

C. Overlaps between states

For states $|\psi\rangle , |\psi'\rangle \in \{|00\rangle , |01\rangle , |10\rangle , |11\rangle\}$, the overlaps have the form

$$\langle\psi'(0)|\psi(t)\rangle = (-1)^s \frac{e^{\mathrm{i}\alpha(t)}}{\sqrt{\mathcal{N}\mathcal{N}(t)}} \langle 0| \prod_k d_k^\dagger (d_1)^{n_1'} (d_2)^{n_2'} (d_1^\dagger(t))^{n_1} (d_2^\dagger(t))^{n_2} \prod_k d_k(t) |0\rangle . \tag{S12}$$

The minus sign is due to reversing the order of the operators in $\langle\psi'|$ and $s = (n_1' + n_2')(n_1' + n_2' - 1)/2 + N(N-1)/2$. The vacuum overlap can now be calculated using Wick's theorem [7, 8],

$$\langle\psi'(0)|\psi(t)\rangle = (-1)^s \frac{e^{\mathrm{i}\alpha(t)}}{\sqrt{\mathcal{N}\mathcal{N}(t)}} \mathrm{pf}(M). \tag{S13}$$

The matrix M is an anti-symmetric matrix constructed from the contractions between operators, and $\mathrm{pf}(\,\cdot\,)$ is the Pfaffian. The resulting matrix is [7, 9, 10]

$$M = \begin{pmatrix} V^T(0)U(0) & V^T(0)V^*(0) & V^T(0)U(t) & V^T(0)V^*(t) \\ & U^\dagger(0)V^*(0) & U^\dagger(0)U(t) & U^\dagger(0)V^*(t) \\ & & V^T(t)U(t) & V^T(t)V^*(t) \\ & & & U^\dagger(t)V^*(t) \end{pmatrix}. \tag{S14}$$

Note that rows and columns corresponding to unoccupied modes must be truncated [7]. The lower triangle is found using anti-symmetry. For transition probabilities, Eq. (S13) simplifies to

$$|\langle\psi'(0)|\psi(t)\rangle|^2 = \frac{1}{\mathcal{N}\mathcal{N}(t)} |\det(M)|. \tag{S15}$$

SUPPLEMENTARY SECTION 2: TIME-DEPENDENT GATE PROTOCOLS

In order to implement time-dependent gate protocols, we use the function

$$s(t,t_0) = \frac{\pi}{2}\begin{cases} 0, & t < t_0 \\ \sin^2\left(\frac{t-t_0}{T_\mathrm{R}}\right), & t_0 \le t \le t_0 + T_\mathrm{R} \\ 1, & t > t_0 + T_\mathrm{R} \end{cases} \tag{S16}$$

in order to rotate a spin over a rotation period T_R, starting at time t_0. We choose this function as it allows a smooth transition from 0 to $\pi/2$ for the polar angle. Here, we use spherical coordinates to describe each spin's orientation in space, such that

$$\mathbf{S}_\mathbf{R}(t) = \begin{pmatrix} \cos(\phi(\mathbf{R},t)\cdot\sin(\theta(\mathbf{R},t)) \\ \sin(\phi(\mathbf{R},t)\cdot\sin(\theta(\mathbf{R},t)) \\ \cos(\theta(\mathbf{R},t)) \end{pmatrix}. \tag{S17}$$

The azimuthal angle ϕ is measured with respect to the x-axis. Moreover, ΔT_R is the delay time between the start of one rotation and that of the subsequent rotation on the next site, and ΔT_wait denotes a pause between steps in the gate process. Such a pause ensures that the system equilibrates between steps in the gate process.

A. Gate Protocol for implementing a $\sqrt{\sigma_z}$-gate in the T-Structure

To implement a $\sqrt{\sigma_z}$-gate in the MSH T-structure of Fig. 2 in the main text, we number the sites of the magnetic adatoms from 1 to $2N_x+1$ along the horizontal segment, where N_x is the length of one leg of the T-structure and from $2N_x+1$ to $3N_x$ along the vertical segment. The time dependence of the azimuthal and polar angles of the spins in the network are then given by

$$(\phi_i,\theta_i(t)) = \begin{cases} (\frac{\pi}{2}, \quad -(-1)^i s(t,(i-1)\cdot\Delta T_\mathrm{R}) + (-1)^i s(t,(4N_x+2-i)\cdot\Delta T_\mathrm{R}), & 1\le i\le N_x \\ (\frac{\pi}{2}, \quad 0), & i = N_x+1 \\ (\frac{\pi}{2}, \quad -(-1)^i s(t,(4N_x+2-i)\cdot\Delta T_\mathrm{R}) + (-1)^i s(t,(4N_x+1+i)\cdot\Delta T_\mathrm{R})), & N_x+2\le i\le 2N_x+1 \\ (0, \quad (-1)^i s(t,(i-N_x-1)\cdot\Delta T_\mathrm{R}) - (-1)^i s(t,(7N_x+3-i)\Delta T_\mathrm{R})), & 2N_x+2\le i\le 3N_x+1 \end{cases}. \tag{S18}$$

B. Gate Protocol for implementing a σ_z-gate in the MSH loop-structure

In the MSH loop-structure, we label the magnetic adatoms starting from the lower left corner as 1 and go counter-clockwise up until $4N_x$, where N_x+1 is the number of adatoms on one side of the square. We execute a σ_z gate in two steps: In the first step, we sequentially rotate the adatoms on the lower right half of the loop into the plane starting from the lower left corner, while simultaneously rotating the upper left half out of the plane starting from the upper right corner. In the second step, we go back to the initial configuration by reversing this process, i.e. rotating the spins in the lower right half of the loop back out of the plane starting from the lower left corner, and rotating the spins in the upper left half into the plane starting from the upper right corner. The azimuthal and polar angles for the spins of these $4N_x$ magnetic adatoms are given as a function of time by

$$(\phi_i,\theta_i(t)) = \begin{cases} \left(\frac{\pi}{2}, -s(t,0) + s(t,2N_x\cdot\Delta T_\mathrm{R})\right), & i=1 \\ \left(\frac{\pi}{2}, (-1)^i s(t,(i-1)\cdot\Delta T_\mathrm{R}) - (-1)^i s(t,(2N_x-2+i+\Delta T_\mathrm{R})\cdot\Delta T_\mathrm{R})\right), & 1< i\le N_x \\ \left(0, -(-1)^i s(t,(i-1)\cdot\Delta T_\mathrm{R}) + (-1)^i s(t,(2N_x-2+i)\cdot\Delta T_\mathrm{R}+\Delta T_\mathrm{wait})\right), & N_x+1\le i\le 2N_x \\ (0, -s(t,T_\mathrm{R}+2N_x\cdot\Delta T_\mathrm{R}+\Delta T_\mathrm{wait}) + s(t,T_\mathrm{R}+(4N_x-1)\cdot\Delta T_\mathrm{R}+\Delta T_\mathrm{wait})), & i=2N_x+1 \\ \left(\frac{\pi}{2}, -(-1)^i s(t,(i-2N_x-1)\cdot\Delta T_\mathrm{R}) + (-1)^i s(t,(i-1)\cdot\Delta T_\mathrm{R}+\Delta T_\mathrm{wait})\right), & 2N_x+1\le i\le 3N_x \\ \left(0, (-1)^i s(t,(i-2N_x-1)\cdot\Delta T_\mathrm{R}) - (-1)^i s(t,(i-1)\cdot\Delta T_\mathrm{R}+\Delta T_\mathrm{wait})\right), & 3N_x+1\le i\le 4N_x \end{cases}. \tag{S19}$$

C. Gate Protocol for implementing a σ_x-gate in the MSH double loop-structure

In order to implement a σ_x-gate in the MSH double loop structure shown in Fig. 3 in the main text, we label the adatom sites from 1 to $8N_x$, where N_x+1 is the number of adatoms along one side of each square. The sites 1 to $4N_x$ are on the lower left square, starting from the lower left corner going counter-clockwise, and the sites $4N_x+1$ to $8N_x$ are on the upper right square, again starting at the lower left corner and going counterclockwise. The crossings of the two squares occurs at sites N_x+1+d and $3N_x+1-d$ in the first square and at sites $5N_x+1-d$ and $7N_x+1+d$ in the second square, where d is both the horizontal and vertical distance from the lower left corner of the first square to the lower left corner of the second square. The azimuthal and polar angles of the gate process are then given by

$$
(\phi_i,\theta_i(t)) =
\begin{cases}
\left(\frac{\pi}{2}, s(t,N_x\cdot\Delta T_{\mathrm{R}}) - s(t,8N_x\cdot\Delta T_{\mathrm{R}}+4\Delta T_{\mathrm{wait}})\right), & i=1\\
\left(\frac{\pi}{2}, (-1)^i s(t,(i-1)\cdot\Delta T_{\mathrm{R}}) - (-1)^i s(t,(i-1+N_x)\cdot\Delta T_{\mathrm{R}})\right), & 1<i\leq N_x\\
\left(0, (-1)^i s(t,(i-1)\cdot\Delta T_{\mathrm{R}}) - (-1)^i s(t,(i+3N_x)\cdot\Delta T_{\mathrm{R}}+2\Delta T_{\mathrm{wait}})\right), & N_x<i\leq 2N_x, i\neq N_x+1+d\\
\left(0, f_{Nx+1+d}(t)\right), & i=N_x+1+d\\
\left(\frac{\pi}{2}, s(t,2N_x\cdot\Delta T_{\mathrm{R}}) - s(t,7N_x\cdot\Delta T_{\mathrm{R}}+4\Delta T_{\mathrm{wait}})\right), & i=2N_x\\
\left(\frac{\pi}{2}, (-1)^i s(t,(i+2N_x-1)\cdot\Delta T_{\mathrm{R}}+2\Delta T_{\mathrm{wait}}) - (-1)^i s(t,(i+5N_x)\cdot\Delta T_{\mathrm{R}}+4\Delta T_{\mathrm{wait}})\right), & 2N_x+1<i\leq 3N_x, i\neq 3N_x+1-d\\
\left(\frac{\pi}{2}, f_{3Nx+1-d}(t)\right), & i=3N_x+1-d\\
\left(0, -(-1)^{3N_x} s(t,(5N_x)\cdot\Delta T_{\mathrm{R}}+2\Delta T_{\mathrm{wait}}) + (-1)^{3N_x} s(t,8N_x\cdot\Delta T_{\mathrm{R}}+4\Delta T_{\mathrm{wait}})\right), & i=3N_x+1\\
\left(0, -(-1)^i s(t,(i-3N_x-1)\cdot\Delta T_{\mathrm{R}}) + (-1)^i s(t,(i+4N_x-1)\cdot\Delta T_{\mathrm{R}}+4\Delta T_{\mathrm{wait}})\right), & 3N_x+1<i\leq 4N_x\\
\left(\frac{\pi}{2}, -s(t,4N_x\cdot\Delta T_{\mathrm{R}}+\Delta T_{\mathrm{wait}}) + s(t,(6N_x+1)\cdot\Delta T_{\mathrm{R}}+3\Delta T_{\mathrm{wait}})\right), & i=4N_x+1\\
\left(\frac{\pi}{2}, s(t,(i+N_x-1)\cdot\Delta T_{\mathrm{R}}+3\Delta T_{\mathrm{wait}}) - s(t,(i+2N_x)\cdot\Delta T_{\mathrm{R}}+3\Delta T_{\mathrm{wait}})\right), & 4N_x+1<i\leq 5N_x, i\neq 5N_x+1-d\\
\left(0, -(-1)^i s(t,(i-3N_x)\cdot\Delta T_{\mathrm{R}}+\Delta T_{\mathrm{wait}}) + (-1)^i s(t,(i+N_x-1)\cdot\Delta T_{\mathrm{R}}+3\Delta T_{\mathrm{wait}})\right), & 5N_x<i\leq 6N_x\\
\left(\frac{\pi}{2}, (-1)^i s(t,(i-4N_x-1)\cdot\Delta T_{\mathrm{R}}+\Delta T_{\mathrm{wait}}) - (-1)^i s(t,(i-3N_x)\cdot\Delta T_{\mathrm{R}}+\Delta T_{\mathrm{wait}})\right), & 6N_x<i\leq 7N_x\\
\left(0, (-1)^i s(t,(i-4N_x-1)\cdot\Delta T_{\mathrm{R}}+\Delta T_{\mathrm{wait}}) - (-1)^i s(t,(i-2N_x)\cdot\Delta T_{\mathrm{R}}+3\Delta T_{\mathrm{wait}})\right), & 7N_x<i\leq 8N_x, i\neq 7N_x+1+d
\end{cases}
\tag{S20}
$$

For the two crossing points of the squares we defined

$$
\begin{aligned}
f_{Nx+1+d}(t) = & -(-1)^{N_x+d} s(t,(N_x+d)\cdot\Delta T_{\mathrm{R}}) + (-1)^{N_x+d} s(t,(4N_x+d+1)\cdot\Delta T_{\mathrm{R}}+2\Delta T_{\mathrm{wait}})\\
& -(-1)^{N_x+d} s(t,(6N_x-d)\cdot\Delta T_{\mathrm{R}}+3\Delta T_{\mathrm{wait}}) + (-1)^{N_x+d} s(t,(7N_x-d+1)\cdot\Delta T_{\mathrm{R}}+3\Delta T_{\mathrm{wait}})\\
f_{3Nx+1-d}(t) = & -(-1)^{3N_x-d} s(t,(3N_x+d)\cdot\Delta T_{\mathrm{R}}+\Delta T_{\mathrm{wait}}) + (-1)^{3N_x-d} s(t,(8N_x-d+1)\cdot\Delta T_{\mathrm{R}}+4\Delta T_{\mathrm{wait}})\,.
\end{aligned}
$$

MZM Distance	μ [t_e]	$\frac{1}{\Delta E_{11}-\Delta E_{00}}$ [τ_e]	T_{0011} [τ_e]	$\frac{1}{\Delta E_{10}-\Delta E_{01}}$ [τ_e]	T_{0110} [τ_e]
10	-3.5	32.08025026	28.5	60.4664097	53
10	-3.55	49.24301723	36.5	61.62151436	93
10	-3.6	77.61149389	62	152.1714373	70
10	-3.707204	51.21434972	420	14184.5468	90
14	-3.36	115.7405706	100	327.3998397	90
14	-3.470485	737.9277107	200	738.0488102	480
14	-3.45805	532.7488345	350	534083.6629	155

Supplementary Table I. Initial energy differences (at $t = 0$) between the many-body states in the even and odd parity sectors for the double-loop MSH structure and the oscillation periods in the transition probabilities. Parameters are $(\alpha, \Delta, J) = (0.9, 2.4, 5.2)t_e$, and $\Delta T_\mathrm{R} = 0.1T_\mathrm{R}$.

SUPPLEMENTARY SECTION 3: OSCILLATIONS IN THE TRANSITION PROBABILITIES $p_{e,o}$

The oscillatory dependence of $p_{e,o}$ on the characteristic time scale of the gate process was previously suggested [4, 6, 11, 12] to arise from a finite energy splitting between the two many-body states within each parity sector. Such a splitting originates from the finite hybridization between the MZMs in systems whose size is not significantly larger than the MZM localization length; the latter being given by the superconducting coherence length, ξ_c, along the network direction. In Supplementary Table I we present a series of cases where we compare the inverse energy splitting in the initial state, and the observed oscillation period. Here, we denote the oscillation period of the transition amplitude between the $|00\rangle$ and $|11\rangle$ states by T_{0011} and the oscillation period of the transition amplitude between the $|01\rangle$ and $|10\rangle$ states by T_{0110}. While we find in general that a decrease in the energy splitting leads to an increase in the oscillation period, there also exist exceptions to this behavior. The reason that the oscillation period cannot in general be directly tied to the initial inverse energy splitting is that this energy splitting itself changes significantly as a function of time during the gate process, as shown in Supplementary Fig. 1 for 4 representative cases.

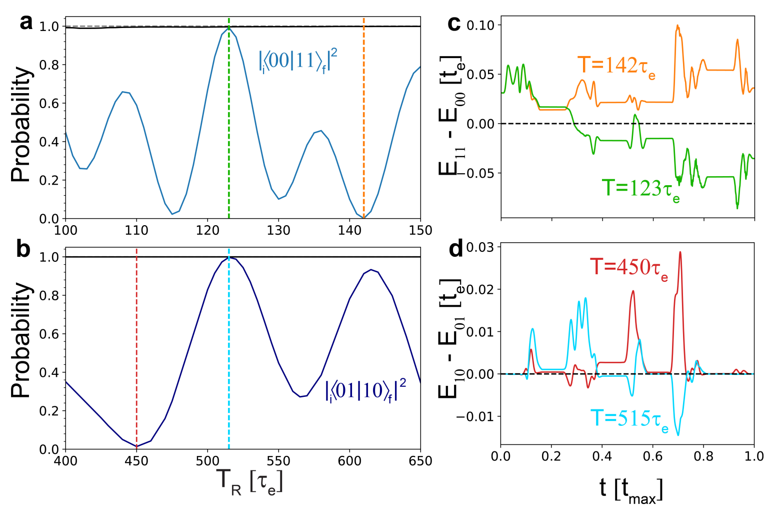

Supplementary Figure 1. Transition probabilities in **a** the even parity sector for $\mu = -3.5t_e$, and **b** the odd-parity sector with $\mu = -3.45805t_e$ on the double-loop MSH structure of Fig. 4 of the main text. Time-evolved energy differences in the **c** even and **d** odd parity sector at the respective minimum and maximum in the transition probabilities from **a,b**, see dashed lines.

1. REFERENCES

[1] P. Ring and P. Schuck, The Nuclear Many-Body Problem, 1st ed., 1864-5879 (Springer Berlin, Heidelberg, 1980).
[2] J. Alicea, Y. Oreg, G. Refael, F. von Oppen, and M. P. A. Fisher, Non-Abelian statistics and topological quantum information processing in 1D wire networks, Nature Phys **7**, 412 (2011).

[3] H. Shi and S. Zhang, Many-body computations by stochastic sampling in Hartree-Fock-Bogoliubov space, Phys. Rev. B **95**, 045144 (2017).
[4] M. Cheng, V. Galitski, and S. Das Sarma, Nonadiabatic effects in the braiding of non-Abelian anyons in topological superconductors, Phys. Rev. B **84**, 104529 (2011).
[5] C. S. Amorim, K. Ebihara, A. Yamakage, Y. Tanaka, and M. Sato, Majorana braiding dynamics in nanowires, Phys. Rev. B **91**, 174305 (2015).
[6] T. Sanno, S. Miyazaki, T. Mizushima, and S. Fujimoto, Ab Initio simulation of non-Abelian braiding statistics in topological superconductors, Phys. Rev. B **103**, 054504 (2021).
[7] G. F. Bertsch and L. M. Robledo, Symmetry Restoration in Hartree-Fock-Bogoliubov Based Theories, Phys. Rev. Lett. **108**, 042505 (2012).
[8] B. M. Terhal and D. P. DiVincenzo, Classical simulation of noninteracting-fermion quantum circuits, Phys. Rev. A **65**, 032325 (2002).
[9] B. G. Carlsson and J. Rotureau, New and Practical Formulation for Overlaps of Bogoliubov Vacua, Phys. Rev. Lett. **126**, 172501 (2021).
[10] H.-K. Jin, R.-Y. Sun, Y. Zhou, and H.-H. Tu, Matrix product states for Hartree-Fock-Bogoliubov wave functions, Phys. Rev. B **105**, L081101 (2022).
[11] M. S. Scheurer and A. Shnirman, Nonadiabatic processes in Majorana qubit systems, Phys. Rev. B **88**, 064515 (2013).
[12] F. Harper, A. Pushp, and R. Roy, Majorana braiding in realistic nanowire Y-junctions and tuning forks, Phys. Rev. Research **1**, 033207 (2019).